Available on CMS information server

CMS NOTE 2006/114

The Compact Muon Solenoid Experiment

CMS Note

Mailing address: CMS CERN, CH-1211 GENEVA 23, Switzerland

30th June 2006

Search for a Light Standard Model Higgs Boson in the $\mathrm{H} \to \mathrm{WW}^{(*)} \to \mathrm{e}^{+}\nu\mathrm{e}^{-}\bar{\nu}$ Channel

F. Beaudette [a)], C. Charlot [a)], E. Delmeire[*] [a)] [b)], C. Rovelli [c)], Y. Sirois [a)]

a) Laboratoire Leprince-Ringuet, Ecole Polytechnique and IN2P3-CNRS, Palaiseau, France

b) Fellow Swiss National Science Fund, Bern Switzerland

c) Università di Milano Bicocca and INFN Milano, Milano, Italy

Abstract

A prospective analysis for the discovery of a light Standard Model Higgs boson in the CMS experiment at the Large Hadron Collider is presented. The analysis focuses on the inclusive single production $\mathrm{p} + \mathrm{p} \to \mathrm{H} + \mathrm{X}$ and the Higgs boson decay channel $\mathrm{H} \to \mathrm{WW}^{(*)} \to \mathrm{e}^{+}\nu\mathrm{e}^{-}\bar{\nu}$, for a mass M_{H} in the range $120 < M_{\mathrm{H}} < 160$ GeV$/c^2$. A full simulation of the detector response is performed and emphasis is put on the use of detailed electron reconstruction, as well as on realistic treatment of background contamination and systematics. A Standard Model Higgs boson of mass $M_{\mathrm{H}} \gtrsim 134$ GeV$/c^2$ would be observed with a significance above 3 standard deviations in the $\mathrm{e}^{+}\nu\mathrm{e}^{-}\bar{\nu}$ channel alone for an integrated luminosity above 30 fb^{-1}.

[*)] Now at the Universidad Autónoma de Madrid.

1 Introduction

The Standard Model (SM) of electroweak interactions contains a unique physical Higgs boson whose mass, $M_{\rm H}$, is a free parameter of the model. Direct searches for the SM Higgs particle at the LEP $\rm e^+e^-$ collider have lead to a strict lower mass bound of 114.4 GeV$/c^2$ (95% CL) [1]. Ongoing direct searches at the TeVatron $\rm p\bar{p}$ collider by the D0 and CDF experiments could allow for a SM Higgs boson discovery up to $M_{\rm H} \simeq 120$ GeV$/c^2$ [2]. The Higgs boson enters in radiative corrections to electroweak observables. A consistency fit of electroweak precision data carried out in the SM framework results in an indirect constraint of $M_{\rm H} < 237$ GeV$/c^2$ (95% CL) [1].

The inclusive single production reaction $\rm p + p \rightarrow H + X$ followed by the decay $\rm H \rightarrow WW^{(*)} \rightarrow l^+\nu l^-\bar{\nu}$ can provide at the LHC $\rm pp$ collider a sensitivity over the full range of $M_{\rm H}$ favoured by direct and indirect constraints. In the intermediate mass range $2M_{\rm W} \leq M_{\rm H} \leq 2M_{\rm Z}$ where the branching ratio of the SM Higgs boson into a $\rm W$ pair is close to one, the $\rm WW$ channel has been established to be a main discovery channel at the LHC [3, 4]. In this paper, a dedicated strategy is presented for the CMS experiment to improve the sensitivity for a Higgs boson in the lower mass region of $M_{\rm H} < 2M_{\rm W}$ where the $\rm WW^*$ channel is likely to be complemented by measurements in the $\rm ZZ^*$ channel. The present analysis focuses on cases where both the real $\rm W$ and the virtual $\rm W^*$ decay into an electron and a neutrino: $\rm H \rightarrow WW^* \rightarrow e^+\nu e^-\bar{\nu}$ (in short $\rm H \rightarrow 2e2\nu$). The analysis makes use of a detailed simulation of the CMS detector response. A description of the CMS detector can be found elsewhere [5, 6].

This paper is organized as follows. First an overview of the signal and the backgrounds is presented in Section 2. The Section 3.1 then describes the event reconstruction with a particular attention to the isolated electron measurements and identification. The event selection is discussed in Section 4 and possible sources of systematics are identified and studied in Section 5. Finally, the performance is studied in terms of signal over background ratio (S/B) and significance in Section 6.

2 Signal and background simulations

The signal topology is characterized by two oppositely charged electrons at central pseudorapidities (η), large missing energy and no hard jet activity. Because the Higgs boson is a scalar, the $\rm W$ vector bosons are produced with anti-correlated spin projections and the decay electrons tend to be emitted collinear. Below the threshold for real $\rm W$ pair production, the effect is less pronounced due to the virtuality of one (or both) of the $\rm W$ bosons. In this low mass region, the mean properties of kinematic observables for the signal depend on the $M_{\rm H}$ hypothesis. Moreover, electron reconstruction issues become more critical due to the presence of at least one low P_T electron, generally coupled to a virtual boson $\rm W^*$.

All sources of multi-lepton final states and missing transverse energy are potential background sources to the Higgs boson $\rm 2e2\nu$ signal. Processes involving the production of real or virtual vector boson pairs are particularly relevant. This includes direct electroweak production of $\rm WW^{(*)}$, $\rm ZW$ and $\rm ZZ$ pairs, as well as the indirect $\rm W$ production via the top quark decay $\rm t \rightarrow Wb$, in associated $\rm Wt(b)$ and $\rm t\bar{t}$ pair production processes. The Drell-Yan production of $\rm e^+e^-$ pairs where the intermediate $\gamma^*/\rm Z^*$ recoils against a jet has a topology similar to the signal if apparent missing transverse energy arises from a mis-measurement. Finally a ”fake” di-electron with a missing transverse energy final state can be obtained in W+jet(s) events if one jet component is misidentified as an electron.

The $\rm pp$ events for the signal and background production as well as showering processes from partonic final states are generated in PYTHIA [7]. For the $\rm t\bar{t}$ and $\rm Wt(b)$ production, PYTHIA has been interfaced with the event generator TopReX [8]. The generator level leading order (LO) cross sections are corrected for next-to-leading order (NLO) effects. One exception concerns the $\rm gg \rightarrow WW^{(*)}$ component of the $\rm WW^{(*)}$ continuum background which is generated at LO using a matrix-element program [9] linked to PYTHIA.

All $\rm W$ bosons are forced into an $\rm e\nu$ final state. The contamination from $\rm W$ boson decays into $\tau\nu$ final states with subsequent $\tau \rightarrow e\nu\nu$ decays is small given the small branching ratio of the latter. The inclusion of $\tau\nu e\nu$ and $2\tau 2\nu$ final states would increase both the Higgs boson signal and the background by about 10%.

The generated events are subject to a full GEANT based simulation of the CMS detector response [10] and reconstructed in detail using the CMS ORCA software [11]. The fast simulation FAMOS [12] of the CMS detector has also been used to determine the efficiency of the kinematic cuts in the specific case of the Z+jet(s) background.

2.1 Higgs boson signal

The generated signal events comprise the main SM Model Higgs boson production processes at the LHC: gluon fusion $\rm gg \rightarrow H$ and Vector Boson Fusion (VBF) $\rm qq \rightarrow qqH$. Feynman diagrams for these processes are presented in Fig. 1. An event-by-event re-weighting using K-factors depending on the Higgs boson transverse momentum is applied to the signal events resulting from gluon fusion. The re-weighting factors are extracted from the ratio of the MC@NLO [13] and the PYTHIA predictions for the Higgs boson transverse momentum [14]. The total cross

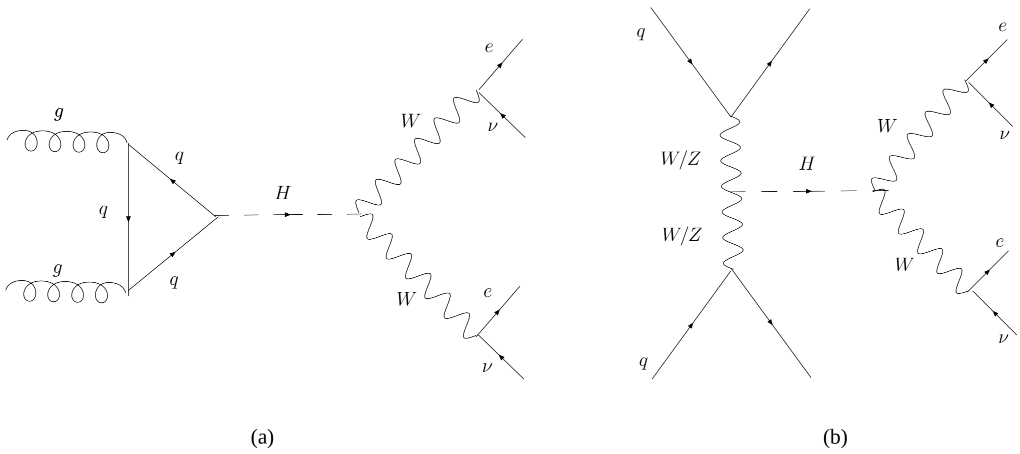

Figure 1: *The dominant hard processes for Standard Model Higgs boson production at the LHC* pp *collider;* a) *gluon fusion* $\mathrm{gg} \to \mathrm{H}$, b) *Vector Boson Fusion (VBF)* $\mathrm{qq} \to \mathrm{qqH}$.

M_{H} (GeV/c^2)	$\sigma_{\mathrm{gg}}^{NLO}$ (pb)	σ_{VBF}^{NLO} (pb)	BR(H → WW$^{(*)}$) (%)	$\sigma_{tot}^{NLO} \times$ BR^2(W → eν) (fb)
120	36.5	4.47	13	63
130	31.7	4.14	29	119
140	27.8	3.83	49	176
150	24.6	3.56	68	221

Table 1: *The NLO cross section for the* $\mathrm{H} \to \mathrm{WW}^{(*)} \to 2\mathrm{e}2\nu$ *signal as function of the Higgs boson mass* M_{H}.

section for the SM Model Higgs boson production is rescaled to the NLO cross section calculated by M.Spira [15] using the CTEQ6M structure functions [16] and a 175 GeV$/c^2$ top quark mass. The NLO effects increase the contribution of the gluon fusion to the cross section by about a factor 2, while the contribution of the VBF remains essentially unchanged. Table 1 gives the cross section for Higgs boson production through gluon fusion and VBF separately. The total NLO cross section for the signal process as well as the branching ratio's for $\mathrm{H} \to \mathrm{WW}^{(*)}$, calculated with HDECAY [17] are also quoted.

2.2 Backgrounds

The NLO cross sections for the background processes are given in Table 2. The dominant irreducible background is the $\mathrm{WW}^{(*)}$ continuum. The W pairs are produced through t-channel quark exchange processes or via gg induced box diagrams as shown in Fig. 2. A similar re-weighting as for the Higgs boson signal is performed

Background Process	σ^{NLO} (fb)
W+jet(s) → eν + jet(s)	5 900 000
Z+jet(s) → e$^+$e$^-$ + jet(s)	822 000
$\mathrm{t\bar{t}} \to 2\mathrm{e}2\nu\mathrm{bb}$	9700
$\mathrm{tWb} \to 2\mathrm{e}2\nu\mathrm{bb}$	380
$\mathrm{qq} \to \mathrm{WW}^{(*)} \to 2\mathrm{e}2\nu$	1300
$\mathrm{gg} \to \mathrm{WW}^{(*)} \to 2\mathrm{e}2\nu$	50 (LO)
$\mathrm{ZW} \to \mathrm{e}^+\mathrm{e}^-\mathrm{X}$	480
$\mathrm{ZZ} \to 2\mathrm{e}2\nu$	230

Table 2: *The NLO cross section of the background processes. For the* $\mathrm{W/Z}$*+jet(s) processes, the phase space is restricted to* $M(\mathrm{Z}/\gamma^*) >$ *12 GeV/*c^2*. The valid range for the* Z*+jet(s) sample is 20 GeV/*$c <$ $P_T(\mathrm{Z}/\gamma^*)$ *<250 GeV/*c *and 20 GeV/*$c <$ $P_T(\mathrm{W}) < 300$ *GeV/c for the* W*+jet(s) sample. The* $\mathrm{gg} \to \mathrm{WW}^{(*)}$ *process cross section is at LO only.*

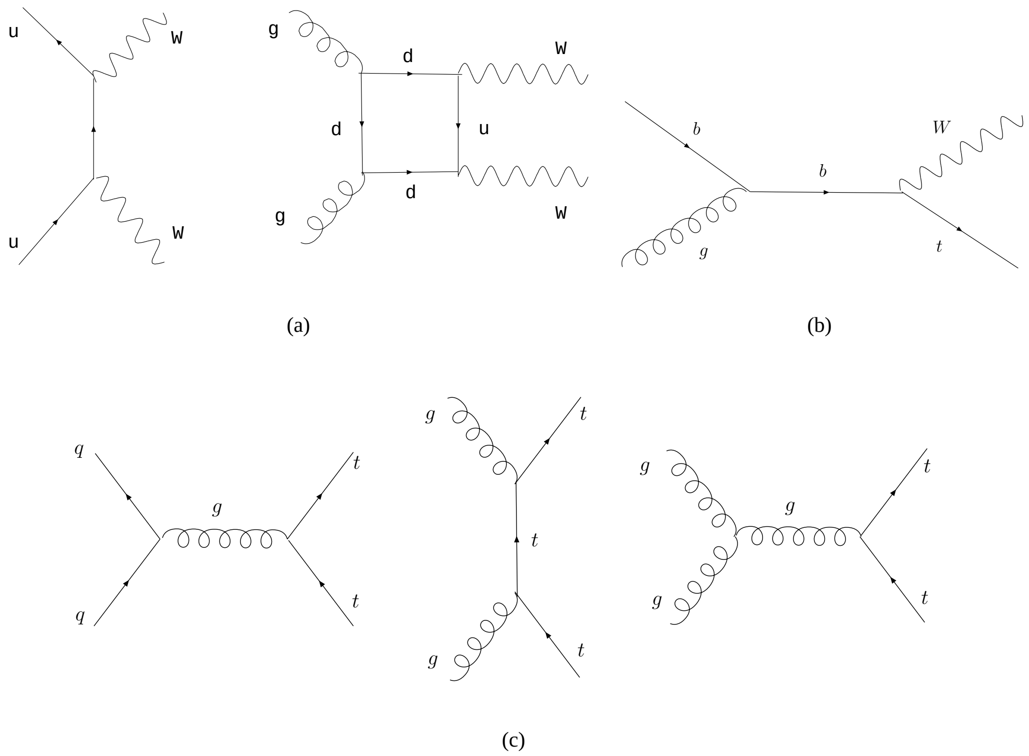

Figure 2: *Some background processes to the Higgs boson production in the decay mode* $\mathrm{H} \rightarrow \mathrm{WW}^{(*)} \rightarrow 2\mathrm{e}2\nu$; a) $\mathrm{WW}^{(*)}$ *production*, b) *single resonant top production and*, c) *double resonant top production.*

with K-factors that depend on the transverse momentum of the $\mathrm{WW}^{(*)}$ system [4]. The NLO cross section of the $\mathrm{qq} \rightarrow \mathrm{WW}^{(*)}$ process as well as the ZZ and ZW vector boson production have been computed with MCFM and CTEQ6M structure functions [18]. The cross section for the $\mathrm{gg} \rightarrow \mathrm{WW}^{(*)}$ process is known at LO [9].

Another source of W boson pairs is the doubly resonant $\mathrm{t\bar{t}}$ production which proceeds mostly via gluon fusion but also via quark annihilation. The $\mathrm{t\bar{t}}$ background constitutes one of the most important reducible background. The total NLO cross section is 840 pb [19]. This background differs from the signal by the presence of additional high P_T jets from the b quarks in the final state. In single resonant top production, a t quark is produced in association with a real W boson via weak interactions induced by a gluon and an b-quark from the sea inside the proton, $\mathrm{bg} \rightarrow \mathrm{tW}$. The NLO cross section for single top production is 33.4 pb [20]. Feynman diagrams for the top production are presented in Fig. 2.

The inclusive $\mathrm{p + p \rightarrow Z + X}$ and $\mathrm{p + p \rightarrow W + X}$ production processes followed respectively by the decay modes $\mathrm{Z} \rightarrow \mathrm{e^+e^-}$ and $\mathrm{W} \rightarrow \mathrm{e}\nu$ have huge cross sections at the LHC [18, 21]. The LO and NLO cases must be distinguished for the $\mathrm{Z + jet(s)}$ background. The LO Drell-Yan production of electron-positron pairs $\mathrm{q\bar{q}} \rightarrow \mathrm{Z}^{(*)}/\gamma^* \rightarrow \mathrm{e^+e^-}$ is characterized by two almost back-to-back electrons and no missing energy. This topology differs from the signal topology where the electrons are emitted almost collinear and are accompanied by at least two neutrinos leading to a significant missing energy. Such contribution [18] is easily suppressed by cuts on the angular separation between the electrons and on the invariant mass of the $\mathrm{e^+e^-}$ system as will be introduced at analysis level in Section 4.3. Drell-Yan events become more dangerous when the Z^*/γ^* recoils against jets. The boost of the $\mathrm{e^+e^-}$ system closes up the opening angle between the electrons in the laboratory rest frame. Therefore, a filter has been applied to select the events with $20\,\mathrm{GeV}/c < P_T(\mathrm{Z}/\gamma^*) < 250\,\mathrm{GeV}/c$. Significant differences in the cross section between PYTHIA and MCFM have been observed when the di-lepton invariant mass approaches zero. Moreover, for low mass values, other production mechanisms than the Z/γ^* process, like J/ψ production, may dominate and one needs to include additional diagrams in the cross section calculation. Therefore, a lower cut $M(\mathrm{Z}/\gamma^*) > 12$ GeV/c^2 is also applied. In this mass region, a good agreement is obtained between PYTHIA and MCFM.

The relevant cross sections for this analysis at NLO for the $\mathrm{Z + jet(s)}$ and $\mathrm{W + jet(s)}$ backgrounds are given in Table 2.

3 Event Reconstruction

3.1 Electron reconstruction and identification

The reconstruction of electrons uses information from the pixel detector [22], the silicon strip tracker [23], and the electromagnetic calorimeter (ECAL) [24]. These detectors are immersed in a 4 T magnetic field parallel to the collider beam z axis. The reconstruction proceeds in three main steps. First, the energy deposited in the ECAL is collected in superclusters built around seed clusters, themselves containing a seed crystal with a high energy deposition. The superclustering procedure [25] is designed to minimize the energy containment variations for electrons and to collect the bremsstrahlung photons emitted by the electrons while traversing the inner tracker material. Second, the electromagnetic superclusters are used to drive the search for hits in the pixel detector which will serve as seeds for the building of electron tracks. Finally an inward-outward track reconstruction is performed. The electron measurement performances at low transverse momentum is optimized by using the full track-cluster combination proposed in Ref. [26]. The Gaussian Sum Filter algorithm [27] is used for electron track reconstruction to efficiently collect track hits up to the end of the tracker volume in presence of large amount of bremsstrahlung emission.

The electron candidates are required to have a minimal transverse energy measured of the supercluster of $E_T^{\rm sc}$ >10 GeV, and to be within the acceptance $|\eta^{\rm sc}|$ <2.5. A pre-selection is made by imposing in addition the following track-supercluster energy-momentum and geometrical matching [26] requirements:

- $H/E < 0.2$;
- $E/P_{\rm in} < 3$;
- $\Delta\phi_{\rm in} = \mid \phi_{\rm sc} - \phi_{\rm in}^{\rm extrap.} \mid < 0.1$;
- $\Delta\eta_{\rm in} = \mid \eta_{\rm sc} - \eta_{\rm in}^{\rm extrap.} \mid < 0.02$;
- $IP/\sigma_{IP} < 10$;

where $\phi_{\rm in}^{\rm extrap.}$ and $\eta_{\rm in}^{\rm extrap.}$ are the ϕ- and η-coordinates of the track propagated through the magnetic field up to the ECAL, and $\phi_{\rm sc}$ and $\eta_{\rm sc}$ the ϕ- and η-value of the electromagnetic supercluster. The ratio H/E between the energy deposit in the hadronic calorimeter (HCAL) cell behind the seed cluster and the supercluster energy in the ECAL is expected to be small for electrons, and large for hadrons. A loose matching is required between the supercluster energy E and the track momentum at the vertex $P_{\rm in}$. The cut on the transverse impact parameter significance IP/σ_{IP} is imposed to reduce the contamination of secondary electrons from backgrounds with b-quark jets.

More stringent electron identification requirements are then imposed using observables able to discriminate real electrons from fakes ones in QCD jets, originating for instance from $\pi^{\pm}\pi^{0}$ overlaps and γ conversions. To better deal with the different topologies of electrons in the detector, the classification of electron candidates according to their observable characteristics introduced in Ref. [26] is used. The 'golden', 'narrow', 'big brem' and 'showering' classes are considered in this analysis. The following observables are used:

- the shower spread in η
  $$\sigma_{\eta\eta}^2 = \frac{\Sigma_i(\eta_i - \eta_{\rm seed})^2 E_i}{\Sigma_i E_i}$$
  where i runs over the 5x5 matrix around the most energetic crystal (seed). With magnetic field lines aligned with the z axis, the bremsstrahlung photons remain close to the electron track in the (non-bending) r-z plane. As a result, the spread in η is not affected by bremsstrahlung and allows a better discrimination between real electrons and fakes than the spread in ϕ.
- $E_{\rm seed}/P_{\rm out}$
  with $E_{\rm seed}$ the seed cluster energy [25] and $P_{\rm out}$ the estimate of the track momentum at the entrance of ECAL.
- E_9/E_{25}
  the ratio of the energy deposited in a 3x3 and a 5x5 matrix of ECAL crystals around the seed. The variable exploits the fact that electromagnetic showers are narrower than hadronic showers.

- $\Delta\phi_{\rm out} = \mid \phi_{\rm sc} - \phi_{\rm out} \mid$
  where $\phi_{\rm out}$ is the position in ϕ of the track extrapolation at the radius of the estimated supercluster mean depth [26].

A class- and η-dependent set of electron identification cuts has been used to preserve a good efficiency for real electrons while allowing for sufficient rejection of backgrounds when used in combination with electron isolation, as discussed in the Section 3.2.

The supercluster energy corrections as well as the combination of calorimeter and tracking information, proposed in Ref. [26], are used to determine the electron transverse momentum $P_T^{\rm e}$ at vertex.

3.2 Electron isolation

Electron candidates have to be isolated. Isolation criteria based either on tracker- or calorimeter-only information are applied.

First, the electrons are asked to be isolated in the tracker by requiring

$$\sum_{tracks} \frac{P_T^{\rm track}}{P_T^{\rm e}} < 0.05\ .$$

Here the sum runs over the tracks, not identified as electrons, falling in a cone of size $\Delta R = \sqrt{(\Delta\eta)^2 + (\Delta\phi)^2}$ = 0.2 centered on the candidate electron. The tracks entering the sum must furthermore originate from the same vertex as the candidate electron within $\mid z^{\rm \ track} - z^{\rm \ e} \mid <$ 0.2 cm, where $z^{\rm \ track}$ and $z^{\rm \ e}$ are the z coordinates of the tracks at the closest distance of approach to the beam axis.

Second, the information provided by the hadron calorimeter is exploited. All calorimeter towers [6] containing an energy $E^{\rm \ tower} >$2 GeV and falling in the isolation cone with radius ΔR = 0.2, centred on the candidate electron, are considered. The electrons are asked to be isolated from hadronic energy flow measured in the HCAL within calorimeter towers by requiring

$$\sum_{\rm towers} \frac{E_T^{\rm HCAL}}{P_T^{\rm e}} < 0.05\ .$$

The optimization of these isolation cuts has been performed on the W+jet(s) sample with the goal to provide sufficient rejection of “fake” electron candidates from jet misidentification, while preserving a best possible electron detection efficiency.

3.3 Jet reconstruction and Missing Transverse Energy

A reconstruction of jets is fundamental for a powerful rejection of the $\rm t\bar{t}$ background. The Iterative Cone Algorithm [6] is used to reconstruct the jets from the energy deposits in the ECAL and HCAL. A cone size of ΔR = 0.5 is used and calorimeter towers centred within the cone and with $E_T^{\rm tower} > 0.5$ GeV and $E^{\rm \ tower} > 0.8$ GeV are considered in the sum for the jet reconstruction. Only raw jets with $E_T^{\rm jet} > 10$ GeV are kept.

At low $E_T^{\rm jet}$, the distinction between real and fake jets can be improved through the use of a so-called α-parameter [4]. This parameter is constructed as follows: all charged tracks with a transverse momentum $P_T^{\rm track} > 2$ GeV$/c$ and with at least 5 hits, within a radius of $\Delta R < 0.5$ around the jet axis and coming from the same event vertex as the signal electrons ($\mid z^{\rm \ track} - z^{\rm \ vertex} \mid < 0.4$ cm) are collected

$$\alpha = \frac{\sum_{tracks} P_T^{\rm track}}{E_T^{\rm jet}}$$

The mean $z^{\rm e}$ position of the electrons is hereby taken as event vertex $z^{\rm \ vertex}$.

In the analysis, the missing transverse energy (MET), is reconstructed by adding vectorially the transverse energy measured in ECAL and HCAL cells and the transverse energy of the reconstructed muons.

4 Event Selection and Kinematics

4.1 Trigger

First, the $\rm H \rightarrow WW^{(*)} \rightarrow 2e2\nu$ events need to pass the global Level 1 (L1) trigger, followed by the High Level Trigger (HLT). For the analysis, the HLT response is defined as the logical OR of the Single Electron Trigger (one isolated electron candidate with $P_T > 26$ GeV/c) and the Double Electron Trigger (two isolated electron candidates with $P_T > 14.5$ GeV/c). Only a marginal gain on the HLT efficiency for the Higgs boson signal is seen when including the Double Relaxed Electron Trigger (2 isolated electron candidates with $P_T > 21.8$ GeV/c). The number of events passing the full HLT trigger that are exclusively triggered by the Double Relaxed Electron Trigger is of the order of the percent. Tables 7, 8 and 9 give the L1+HLT efficiency for the Higgs signal and for the backgrounds. The efficiency varies from 59% for a Higgs boson signal with $M_{\rm H} = 130$ GeV/c^2 to 66% for $M_{\rm H} = 150$ GeV/c^2.

4.2 Data reduction

First, a data reduction is applied: events that pass the L1+HLT requirements and which contain exactly 2 isolated electrons with $E_T^{\rm e} > 10$ GeV and $\mid \eta^{\rm e} \mid< 2.5$ and coming from the same event vertex ($\mid z^{\rm e+} - z^{\rm e-} \mid < 0.2$ cm) are selected.

A Central Jet Veto (CJV) is then applied against the $\rm t\bar{t}$ and $\rm Wt(b)$ backgrounds. These backgrounds are characterized by high P_T jets initiated by heavy quark flavours which are more centrally distributed than recoil jets in Higgs boson signal events. The CJV consists in rejecting events containing jet(s) emitted in the central region ($\mid \eta^{\rm \ jet} \mid < 2.5$) and with a transverse energy $E_T^{\rm jet} > 20$ GeV. To increase further the rejection power of the CJV, events with jet(s) in the range $15 < E_T^{\rm jet} < 20$ GeV and having $\alpha > 0.2$ are also discarded.

4.3 Basic selection

The kinematic selection is based on a series of cuts chosen to maximize the significance for a signal observation, which demands a good signal over background ratio, while preserving a high signal detection efficiency. The introduction of $M_{\rm H}$-dependent cuts allows to follow the evolution of the event characteristics in the lower range of the Higgs boson mass spectrum. The following kinematic cuts are applied.

- $25 < P_T^{\rm e}(\rm highest) < 50$ GeV/c ;

  where $P_T^{\rm e}(\rm highest)$ is the transverse momentum of the leading electron. The lower threshold is unavoidable to be compatible with the trigger requirements. The higher cut is applied to restrict the analysis to the transverse momentum range expected from W decay.

- $P_T^{\rm e}(\rm lowest) > 15$ GeV/c ;

  where $P_T^{\rm e}(\rm lowest)$ is the transverse momentum of the second electron. The signal for the low $M_{\rm H}$ values considered in this analysis peaks around $P_T^{\rm e} \simeq 20$ GeV/c. The cut position is adjusted as a compromise between signal detection efficiency and the necessity to avoid the contamination from W+jet(s) events as discussed in Section 4.4.2.

- 40 GeV $<$ MET $< M_{\rm H}\, c^2 - 50$ GeV ;

  where the lower cut is applied to reject mainly the $\rm WW^{(*)}$ continuum and the contamination from Drell-Yan events, and the higher cut rejects the $\rm t\bar{t}$ and $\rm Wt(b)$ backgrounds.

- $\Delta\phi(\rm e^+e^-) < 100°$;

  where $\Delta\phi(\rm e^+e^-)$ is the azimuthal angular separation between the electrons. The $\Delta\phi(\rm e^+e^-)$ distribution is expected to peak at small values for the Higgs boson signal while the $\rm e^+$ and $\rm e^-$ for the background are preferably found in opposite hemispheres.

- $12 < M_{\rm ee} < 40$ GeV/c^2 ;

  where $M_{\rm ee}$ is the invariant mass of the $\rm e^+e^-$ system. The lower cut is applied to avoid the contamination of bottomed and charmed mesons, like Υ, J/ψ etc... The higher cut suppresses in particular the Drell-Yan, ZZ and ZW backgrounds which peak around 90 GeV/c^2.

- $M_{\rm H}/2 < M_T(\rm WW) < M_{\rm H}$;

Number of events expected for 10 fb^{-1}	5.9$\times$ 10^7
L1+HLT electron trigger	1.8$\times$ 10^7
pre-selection of $\geq$2 electrons with $P_T^e > 10\,\mathrm{GeV}/c$	2.9$\times$ 10^6
2 identified isolated electrons	2.8$\times$ 10^3

Table 3: *The performance of the electron reconstruction and identification (ID) applied on the* W*+jet(s) background. The number of events expected for 10 fb^{-1} luminosity is given after L1+HLT trigger requirements, electron pre-selection, and final electron ID and isolation cuts.*

with $M_T(\mathrm{WW})$ the reconstructed WW transverse mass defined as

$$\sqrt{2\ P_T(e^+e^-)\ \mathrm{MET}\ (1 - \cos\Delta\phi(\mathrm{MET}, e^+e^-))}$$

with $P_T(e^+e^-)$ the transverse momentum of the e^+e^- system.

The distributions of the basic kinematic observables used for event selection are shown in Fig. 3, for the Higgs boson signal and the backgrounds, together with the optimized cut values. The result and performances of the kinematic selection is given in Tables 7, 8 and 9.

4.4 Reduction of Z+jet(s) and W+jet(s) contamination

After the basic kinematic selection, about one hundred Z+jet(s) events are expected for 10 fb^{-1} of integrated luminosity, compared to less than one hundred events expected for the Higgs boson signal. Hence, the basic kinematic selection has to be complemented. Dedicated cuts are introduced to reduce the contamination from the Z+jet(s) and W+jet(s) backgrounds to a manageable level.

4.4.1 Improved Z+jet(s) rejection

The electrons originating from the decay of the Higgs boson tend to be emitted more centrally than those of the Z decay. This is shown in Fig. 4a where the pseudorapidity distribution of the di-electron system, $\eta(\mathrm{e^+e^-})$, is presented after data reduction.

For the Z+jet(s) background, the observed MET results from mis-measurements of the recoiling jet(s). As a consequence, the MET is preferentially aligned with the hadronic jet at highest E_T^{jet} (leading jet). Moreover this observed MET does not in general balance the P_T of the e^+e^- system. This is in contrast to the expectations for the Higgs boson signal. For the Higgs boson signal events, the MET direction in the transverse plane is in general well separated from the direction of the leading jet (Fig. 4b) and the MET measures well the neutrinos from the W decays (Fig. 4c). Hence, the following cuts are applied:

- $|\ \eta(\mathrm{e^+e^-})\ |<2$;
- $P_T(\mathrm{e^+e^-}) -$ MET $<$ 15 GeV ;
- $\Delta\phi$(MET-leading jet) $> 40°$.

The latter cut is only applied for events in which the leading jet is emitted in the central region ($|\ \eta^{\ jet}\ | < 2.5$) and has $\alpha > 0.2$. These restrictions reduce the sensitivity of the analysis to pile-up or fake jets.

The rejection of the Z +jet(s) events is thus improved by a factor of 2.7. All together, 35 Z +jet(s) events events are expected for 10 fb^{-1}.

4.4.2 Suppression of the W+jet(s) background

The $\mathrm{W+jet(s)} \to \mathrm{e}\nu\mathrm{+jet(s)}$ events where an electron is misidentified in a jet have measured properties similar to those of the Higgs boson signal; two "electrons" and missing transverse energy. Therefore, electron selection plays a major role in the suppression of this background. Table 3 gives the number of $\mathrm{W + jet(s)}$ events that are expected to survive the electron requirements of the L1+HLT trigger, the pre-selection, and the final electron ID (Section 3.1) and isolation (Sections 3.2) cuts, for an integrated LHC luminosity of 10 fb^{-1}. The probability ϵ_{ee} to reconstruct exactly one $\mathrm{e^+e^-}$ pair passing the final electron ID and isolation cuts is 4.7 $\times$ 10^{-5}.

The rejection obtained from these stringent electron requirements is not by itself sufficient to reduce the W+jet(s) contamination to a manageable level. The expected number of events in the whole 20 - 300 GeV P_T region for 10 fb^{-1} of integrated luminosity is 2.8×10^3 prior to the kinematic selection, about $\mathcal{O}(100)\times$ larger

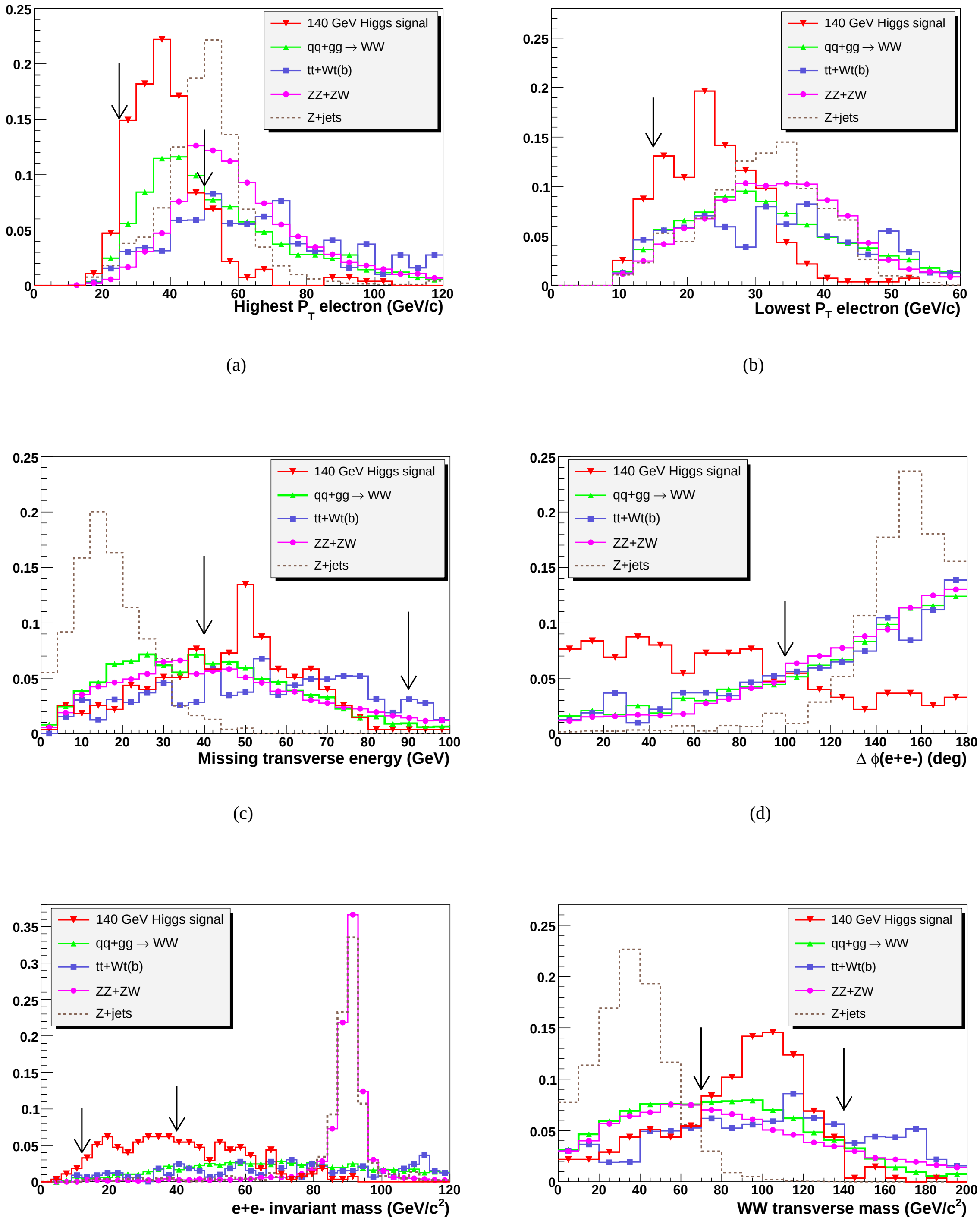

Figure 3: *The shape of the distributions of the kinematic selection variables after data reduction;* a) *transverse momentum of the most energetic electron;* b) *transverse momentum of the second most energetic electron;* c) *missing transverse energy;* d) *angular separation between the electrons in the transverse plane;* e) *invariant mass of the* $\mathrm{e}^+\mathrm{e}^-$ *system;* f) *reconstructed* WW *transverse mass. The vertical arrows indicate the cut positions for the basic 140* GeV/c^2 *Higgs boson signal selection.*

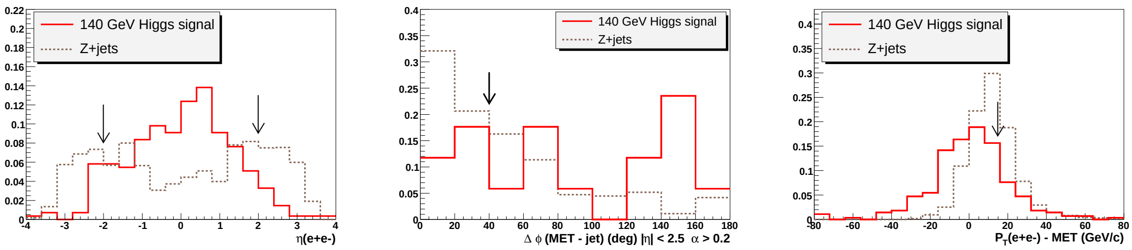

(a) (b) (c)

Figure 4: *Distributions of the* Z*+jet(s) rejection variables after data reduction;* a) *pseudorapidity of the* $\mathrm{e^+e^-}$ *system;* b) *angular separation between the missing transverse energy (MET) direction and the direction of the hadronic jet at highest* E_T^{jet}*;* c) *difference between the transverse momentum of the* $\mathrm{e^+e^-}$ *system and the MET.*

than the expected signal from a Higgs boson of mass $120~\mathrm{GeV}/c^2$. Further rejection is obtained with the basic kinematical cuts introduced in Section 4.3 and the Z+jets cuts described in Section 4.4.1.

Another property of the W+jet(s) events can be exploited. The two electron candidates in the W+jet(s) background tend to be more separated in η than for the Higgs boson signal as shown in Fig. 5. This is because the fake

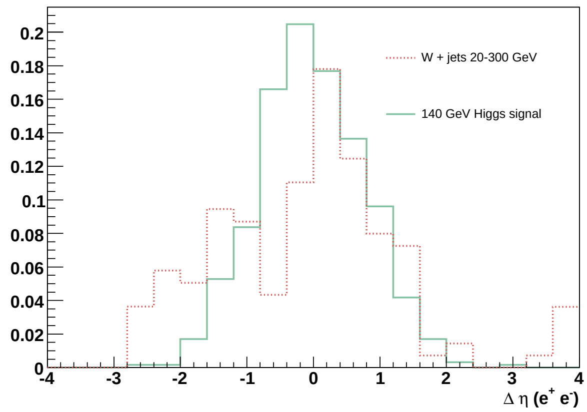

Figure 5: *The separation in pseudorapidity between the two reconstructed electrons* $\Delta\eta(\mathrm{e^+e^-})$*. The distribution is shown for the* W*+jet(s) and the* $140~\mathrm{GeV}/c^2$ *Higgs boson signal samples after pre-selection with a relaxed electron identification.*

electron in W+jet(s) events often appears in low E_T misidentified jet at larger pseudorapidities. Hence, further rejection is obtained by imposing

$$\mid \Delta\eta(e^+e^-) \mid < 1\,.$$

Due to the insufficient statistics of the W+jet(s) sample available for this prospective analysis, the global efficency of the full selection cannot be directly determined. No event survives the full set of electron and kinematic cuts. Therefore a factorization procedure has to be applied.

In a first step, the electron isolation is relaxed by applying only the first five cuts listed in section 3.1 as well as the $E_{\mathrm{seed}}/P_{\mathrm{out}}$ and the isolation criteria, while all other requirements are dropped. It has been checked that the distributions of all the kinematical variables are not affected when the electron identification requirements are thus relaxed. The final efficiency is calculated as the product of the full electron selection efficiency ϵ_{ee}, determined above, and the kinematic cuts efficiency ϵ_{kine} determined using the sample with the relaxed electron identification criteria.

$$\epsilon_{tot} = \epsilon_{\mathrm{ee}} \times \epsilon_{\mathrm{kine}}$$

Conversely, a factorization procedure is used to determine the kinematic cut efficiency ϵ_{kine} by defining five sets of uncorrelated cuts, numbered from 1 to 5, and computing:

$$\epsilon_{\mathrm{kine}} = \epsilon_1 \times \epsilon_2 \times \epsilon_3 \times \epsilon_4 \times \epsilon_5\ .$$

The five sets of cuts are listed below

Set of selection cuts	efficiency (%)
$P_T(e^+e^-) - \mathrm{MET} < 15$ GeV	70
$\mid \Delta\phi(\mathrm{MET} - \mathrm{jet}) \mid > 40°$	74
$\mid \Delta\eta(e^+e^-) \mid < 1$	54
40 GeV < MET < 70 GeV and $M_{\mathrm{H}}/2 < M_T(WW) < M_{\mathrm{H}}$	39
all except above four and CJV	<2

Table 4: *The performance of the kinematic cuts applied on the relaxed electron ID sample.*

- $P_T(e^+e^-) - \mathrm{MET} < 15$ GeV
- $\mid \Delta\phi(\mathrm{MET}\ -\ \mathrm{jet}) \mid > 40°$
- $\mid \Delta\eta(e^+e^-) \mid < 1$
- 40 GeV < MET < 70 GeV and $M_{\mathrm{H}}/2 < M_T(\mathrm{WW}) < M_{\mathrm{H}}$
- all kinematic cuts except the above four and CJV

It has been again checked that the distributions of all the other kinematical variables are not biased when each set of cuts is removed in turn, therefore establishing the validity of the factorization hypothesis.

Since the jet multiplicity is artificially increased when using the relaxed electron identification, the rejection power of the kinematical cuts could be overestimated when including the CJV. This is why the CJV has not been used. This can only result in an underestimate of the final rejection. The fraction, $\epsilon_{i,i=1..5}$ of the W+jets background sample with relaxed electron identification which survive the five sets of kinematic cuts is given in Table 4.

The total efficiency ϵ_{kine} is found to be $< 2.0 \times 10^{-3}$. Altogether, the efficiency on the $\mathrm{W} + \mathrm{jet(s)} \to \mathrm{e}\nu + \mathrm{jets}$ events in the 20-300 GeV/c range is obtained as:

$$\epsilon_{tot} = \epsilon_{\mathrm{ee}} \times \epsilon_{\mathrm{kine}} < (4.7 \times 10^{-5}) \times (2.0 \times 10^{-3}) = 9.3 \times 10^{-8}$$

and the expected number of events for 10 fb^{-1} integrated luminosity is < 6.

4.5 Summary of event selection

Number of events expected for 10 fb^{-1}	M_{H} (GeV/c^2) 120	130	140	150
Signal N_S	11.8	19.0	47.5	54.2
Background N_B	98.3	112.9	124.9	136.3

Table 5: *The number of expected signal and background events for an integrated luminosity of 10* fb^{-1} *as function of Higgs boson mass hypothesis.*

The number of Higgs boson signal and background events expected for an integrated luminosity of 10 fb^{-1} after triggering, electron and kinematic selections is given in Table 5. The expected number of $\mathrm{W/Z}$+jet(s) events are included in the number of background events N_B.

5 Systematics

Beside the luminosity measurement, there are two main sources of uncertainty on the background estimation: experimental and theory uncertainties. The total uncertainty on the background estimation is given by the quadratic sum

$$\Delta N_B = \sqrt{(\Delta\mathcal{L}.\sigma.\epsilon)^2 + (\mathcal{L}.\Delta\sigma.\epsilon)^2 + (\mathcal{L}.\sigma.\Delta\epsilon)^2}$$

Systematics on N_B for 10 fb^{-1}			
	M_{H} (GeV/c^2)		
Sources of systematics	130	140	150
theory	3.9	4.9	5.5
experimental	5.0	7.8	5.2
luminosity	5.6	6.2	6.9
ΔN_B	8.5	11.1	10.2

Table 6: *The contribution of the theory, experimental and luminosity systematics to the background uncertainty estimation for an integrated luminosity of 10* fb^{-1} *as function of Higgs boson mass hypothesis.*

and includes the uncertainty on the luminosity measurement and the uncertainties from theoretical and experimental origin.

Luminosity measurement

For the systematics related to the luminosity measurement, the effect of a 5% uncertainty is taken as systematic uncertainty on the background estimation for luminosities up to 10 fb^{-1} and 3% for luminosities above 30 fb^{-1}, while a linear dependence is used between these points [28].

Theory uncertainties

The $\mathrm{qq} \to \mathrm{WW}^{(*)}$ continuum is normalized with respect to the $\mathrm{Z} \to \mathrm{e}^+\mathrm{e}^-$ signal. The systematic uncertainties coming from the luminosity measurement as well as from the electron and track reconstruction are thus cancelled. The $\sigma(\mathrm{WW})/\sigma(\mathrm{Z})$ ratio is computed in Ref. [30]. The uncertainties linked to the knowledge of the parton density functions and QCD scale uncertainties are 3.6% and 4.5% respectively. The uncertainty coming from the modelling of the spin correlations is deduced from [29] and is found to be about 7%.

The theory uncertainty for the $\mathrm{t\bar{t}}$ background is about 12%. The main contribution comes from the spin correlations modelling, the factorization scale and the parton density functions [19]. The effect of higher order corrections is of minor importance as the CJV tends to favour the production of Higgs bosons of low transverse momentum and therefore reduces the sensitivity to higher order corrections.

For the $\mathrm{gg} \to \mathrm{WW}^{(*)}$ continuum and the $\mathrm{Wt(b)}$ single resonant top background, theory uncertainties of 30%, respectively 20% are taken into account [4]. The ZZ and ZW backgrounds represent only a small fraction of the total expected background and uncertainties of theoretical origin are therefore neglected.

Experimental uncertainties

The effect of the experimental uncertainties on the background evaluation is obtained by varying the relevant observables within their error.

As most of the backgrounds have neutrinos from leptonic W decay in the final state, the MET is expected to be well understood by the comparison of single W events and single Z production where an electron is artificially removed. An uncertainty in the MET resolution of 4.5% and in the MET scale of 2% is expected from studies of the W mass measurement [31] and used to quantify the effect of the uncertainties in the MET measurement.

The MET direction is varied by $7.2°$. Although the MET is mainly related to neutrinos, the uncertainty on the ϕ resolution of the MET for inclusive $\mathrm{t\bar{t}}$ events visible in Figure 20, Chapter 11 of Ref. [6] gives an idea of the order of magnitude of the effect. The jet energy resolution is varied by 2% which corresponds to the uncertainty due to the inhomogeneous calibration of the towers. The jet energy scale is varied by 5%. The uncertainty on the electron energy resolution is taken to be 0.5% in the barrel and 1% in the endcaps as suggested by the ZZ^* analysis. The track reconstruction efficiency is varied by 1% [32] and $1/P_T$ scale is modified by $\pm 0.0005/\mathrm{GeV}$.

The effect on the background estimation of the systematics is shown in Table 6 and is of the order of 6%-7%. For the Z+jet background, only the MET measurement related systematics have been included. The W+jet background only contributes marginally and systematics can be neglected.

6 Results

Tables 7, 8 and 9 summarize the performance of the selection for Higgs masses from 130 GeV/c^2 to 150 GeV/c^2. The expected number of events for is given for 10 fb^{-1} together with the relative efficiency with respect

$M_{\rm H}$ = 130 GeV/c^2 selection	Higgs signal	qq→ WW	gg→ WW	$\rm t\bar{t}$	$\rm Wt(b)$	ZZ	ZW
L1+HLT	696(59%)	8409(64%)	388(73%)	77004(80%)	3057(81%)	1473(61%)	3287(69%)
isolated e^+e^- pair $E_T^{\rm e} > 10$ GeV, $\mid \eta^e \mid < 2.5$	273(39%)	2790(33%)	155(40%)	31435(41%)	1299(42%)	544(37%)	1108(34%)
Central Jet Veto	148(54%)	1817(65%)	131(84%)	1453(5%)	222(17%)	394(72%)	686(62%)
25$<$ $P_T^{\rm e}(\rm highest) < 50$ GeV	120(81%)	854(47%)	61(47%)	309(21%)	50(23%)	108(27%)	223(32%)
$P_T^{\rm e}(\rm lowest) > 15$ GeV	95(79%)	803(94%)	57(94%)	269(87%)	47(94%)	103(96%)	213(96%)
40 $<$ MET $<$ 80 GeV	56(59%)	318(40%)	33(57%)	130(48%)	24(51%)	27(26%)	81(38%)
$\Delta\phi(e^+e^-) < 100°$	45(81%)	222(70%)	28(86%)	90(69%)	16(64%)	12(45%)	23(29%)
12 $< M_{\rm ee} <$ 40 GeV	29.3(64.6%)	74.4(33.5%)	10.5(37.2%)	40.3(45.0%)	5.5(35.2%)	2.6(21.4%)	2.9(12.5%)
$M_{\rm H}/2 < M_T(\rm WW) < M_{\rm H}$	24.7(84.3%)	60.9(81.9%)	6.6(62.7%)	35.9(88.9%)	4.2(77.4%)	2.4(90.9%)	2.6(88.9%
Z+jet(s) cuts	20.7(83.7%)	43.7(71.7%)	5.4(81.2%)	22.4(62.5%)	3.0(70.8%)	1.8(75.0%)	1.8(68.7%)
W+jet(s) cut	19.0(91.7%)	38.5(88.1%)	4.8(89.3%)	22.4(100.0%)	2.6(88.2%)	1.8(100.0%)	1.8(100.0%)
Global efficiency(%)	1.59 $\pm$ 0.29	0.29 $\pm$ 0.03	0.90 $\pm$ 0.13	0.02 $\pm$ 0.01	0.07 $\pm$ 0.02	0.07 $\pm$ 0.02	0.04 $\pm$ 0.01

Table 7: *Performance of the selection optimized for the observation of a Higgs boson signal at a mass of* $130\ {\rm GeV}/c^2$. *The expected number of events for an integrated luminosity of 10* ${\rm fb}^{-1}$ *and the relative efficiency in % (inside the brackets), are given with respect to the previous cut. The global efficiency of the full selection with its statistical uncertainty is also given.*

M_{H} = 140 GeV/c^2 selection	Higgs signal	qq→ WW	gg→ WW	$\mathrm{t\bar{t}}$	$\mathrm{Wt(b)}$	ZZ	ZW
L1+HLT	1122(64%)	8409(64%)	388(73%)	77004(80%)	3057(81%)	1473(61%)	3287(69%)
isolated e^+e^- pair $E_T^{\mathrm{e}} > 10$ GeV, $\mid \eta^e \mid < 2.5$	460(41%)	2790(33%)	155(40%)	31435(41%)	1299(42%)	544(37%)	1108(34%)
Central Jet Veto	230(50%)	1817(65%)	131(84%)	1453(5%)	222(17%)	394(72%)	686(62%)
25$<P_T^{\mathrm{e}}(\mathrm{highest}) <$ 50 GeV	186(81%)	854(47%)	61(47%)	309(21%)	50(23%)	108(27%)	223(32%)
$P_T^{\mathrm{e}}(\mathrm{lowest}) >$ 15 GeV	168(90%)	803(94%)	57(94%)	269(87%)	47(94%)	103(96%)	213(96%)
40 $<$ MET $<$ 90 GeV	106(63%)	331(41%)	36(62%)	139(52%)	27(58%)	28(27%)	83(39%)
$\Delta\phi(e^+e^-) < 100°$	90(85%)	234(71%)	31(87%)	94(68%)	18(66%)	13(47%)	25(30%)
12 $< M_{\mathrm{ee}} <$ 40 GeV	65.0(72.2%)	76.8(32.8%)	11.7(37.8%)	40.3(42.9%)	6.2(34.3%)	2.9(22.0%)	2.9(11.5%)
$M_{\mathrm{H}}/2 < M_T(\mathrm{WW}) < M_{\mathrm{H}}$	63.4(97.4%)	72.0(93.8%)	8.5(73.0%)	35.9(88.9%)	5.1(82.9%)	2.5(87.5%)	2.6(88.9%)
Z+jet(s) cuts	53.4(84.2%)	53.5(74.3%)	7.2(84.3%)	22.4(62.5%)	3.9(75.9%)	1.9(76.2%)	1.9(75.0%)
W+jet(s) cut	47.5(89.1%)	47.9(89.5%)	6.3(88.0%)	22.4(100.0%)	3.5(90.9%)	1.9(100.0%)	1.9(100.0%)
Global efficiency(%)	2.69 $\pm$ 0.36	0.36 $\pm$ 0.03	1.18 $\pm$ 0.14	0.02 $\pm$ 0.01	0.09 $\pm$ 0.02	0.08 $\pm$ 0.02	0.04 $\pm$ 0.01

Table 8: *Performance of the selection optimized for the observation of a Higgs boson signal at a mass of* $140\ \mathrm{GeV}/c^2$. *The expected number of events for a integrated luminosity of 10* fb^{-1} *and the relative efficiency in % (inside the brackets), are given with respect to the previous cut. The global efficiency of the full selection with its statistical uncertainty is also given.*

M_H = 150 GeV/c^2 selection	Higgs signal	qq→ WW	gg→ WW	$\mathrm{t\bar{t}}$	Wt(b)	ZZ	ZW
L1+HLT	1458(66%)	8409(64%)	388(73%)	77004(80%)	3057(81%)	1473(61%)	3287(69%)
isolated e^+e^- pair $E_T^{\mathrm{e}} > 10$ GeV, $\mid \eta^e \mid < 2.5$	603(41%)	2790(33%)	155(40%)	31435(41%)	1299(42%)	544(37%)	1108(34%)
Central Jet Veto	322(53%)	1817(65%)	131(84%)	1453(5%)	222(17%)	394(72%)	686(62%)
25$< P_T^{\mathrm{e}}(\mathrm{highest}) <$ 50 GeV	253(79%)	854(47%)	61(47%)	309(21%)	50(23%)	108(27%)	223(32%)
$P_T^{\mathrm{e}}(\mathrm{lowest}) >$ 15 GeV	235(93%)	803(94%)	57(94%)	269(87%)	47(94%)	103(96%)	213(96%)
40 $<$ MET $<$ 100 GeV	163(69%)	336(42%)	36(63%)	148(55%)	29(63%)	28(27%)	83(39%)
$\Delta\phi(e^+e^-) < 100°$	136(83%)	239(71%)	32(87%)	99(67%)	20(67%)	13(47%)	25(31%)
12 $< M_{\mathrm{ee}} <$ 40 GeV	83.9(61.9%)	80.8(33.8%)	12.0(37.8%)	40.3(40.9%)	7.2(36.6%)	2.9(21.4%)	2.9(11.3%)
$M_{\mathrm{H}}/2 < M_T(\mathrm{WW}) < M_{\mathrm{H}}$	81.4(96.9%)	76.8(95.0%)	10.7(89.6%)	40.3(100.0%)	6.2(85.4%)	2.6(91.7%)	2.6(88.9%)
Z+jet(s) cuts	62.0(76.2%)	57.5(74.9%)	9.3(86.6%)	26.9(66.7%)	4.9(80.0%)	2.0(77.3%)	1.9(75.0%)
W+jet(s) cut	54.2(87.5%)	51.9(90.3%)	8.2(88.7%)	26.9(100.0%)	4.4(89.3%)	2.0(100.0%)	1.9(100.0%)
Global efficiency(%)	2.45 $\pm$ 0.38	0.40 $\pm$ 0.04	1.54 $\pm$ 0.16	0.03 $\pm$ 0.01	0.12 $\pm$ 0.03	0.08 $\pm$ 0.02	0.04 $\pm$ 0.01

Table 9: *Performance of the selection optimized for the observation of a Higgs boson signal at a mass of* $150\ \mathrm{GeV}/c^2$*. The expected number of events for an luminosity of 10* fb^{-1} *and the relative efficiency in % (inside the brackets), are given with respect to the previous cut. The global efficiency of the full selection with its statistical uncertainty is also given.*

$M_{\rm H}$ (GeV/c^2)	S/B	significance for 10 fb^{-1} without sys.	with sys.	with sys. with W/Z+jet(s)
120	0.12	-	-	-
130	0.17	2.1	1.5	1.2
140	0.38	4.8	3.8	2.9
150	0.40	5.1	4.0	3.5

Table 10: *Summary of the significance of the M_H-dependent selection without and with inclusion of the systematics. The effect of the inclusion of the W/Z+jet(s) backgrounds is also given.*

to the previous cut. The global efficiency of the full selection as well as the corresponding statistical uncertainty is also reported.

6.1 Extraction of the signal significance

The estimator S_{cP}, based on the counting method, is chosen to extract the signal significance and calculated using the program [33]. The counting experiment significance S_{cP} is defined as the probability from Poisson distribution with mean N_B to observe equal or greater than $N_S + N_B$ events, converted in equivalent number of sigmas of a Gaussian distribution. The expected number of W+jet(s) and Z+jet(s) events is included in the background sum for the significance estimation as well as the uncertainty on the MET measurement for the Z +jet(s) background. Table 10 shows the S/B ratio and the significance for an integrated luminosity of 10 fb^{-1}.

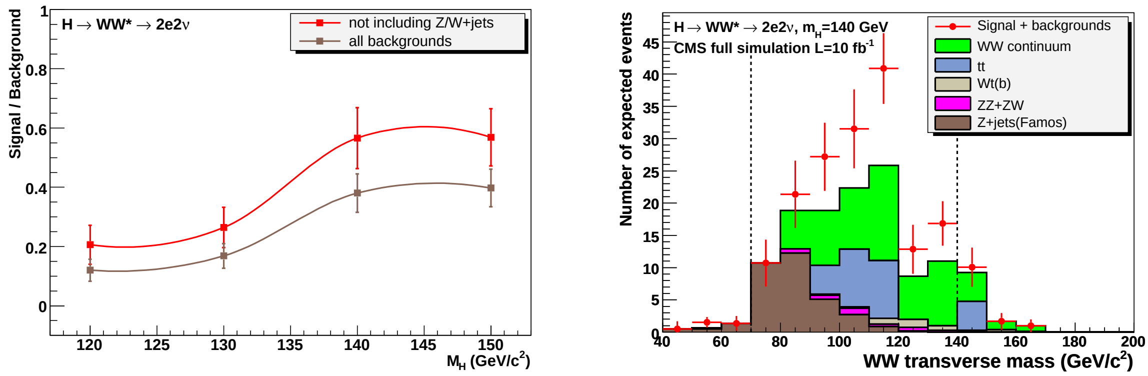

(a) (b)

Figure 6: a) *Signal over background ratio as function of the Higgs boson mass $M_{\rm H}$ with and without inclusion of the expected Z+jet(s) and* W*+jet(s) backgrounds.* b) *Reconstructed* WW *transverse mass distribution for 10* fb^{-1} *integrated luminosity for (the sum of) the background contributions (histograms) and for the signal plus background observation (dots) for a* $140\mathrm{GeV}/c^2$ *Higgs boson signal; the dashed line shows the mass window for the events to enter the significance calculation.*

Figure 6a shows the S/B ratio as function of the Higgs boson mass $M_{\rm H}$. Figure 6b shows the reconstructed WW transverse mass distribution expected in CMS for a typical single experiment with 10 fb^{-1} of integrated luminosity. An excess of event is visible above the sum of background contributions.

Figure 7a shows the significance expected for 30 fb^{-1} of luminosity. A 3σ observation can be achieved for $M_{\rm H}$ $\gtrsim$134 GeV/c^2 with a 30 fb^{-1} luminosity. Figure 7b shows the significance for 60 fb^{-1} of luminosity. A 5σ observation is possible for $M_{\rm H}$ >139 GeV/c^2 given the actual central value of the mean expected background.

7 Conclusions

An optimization of the sensitivity for a light Standard Model Higgs boson in the H $\rightarrow$ WW$^{(*)}$ $\rightarrow$ 2e2ν channel in the mass range 120 $<$ $M_{\rm H}$ $<$ 160 GeV/c^2 has been performed. A particular attention has been

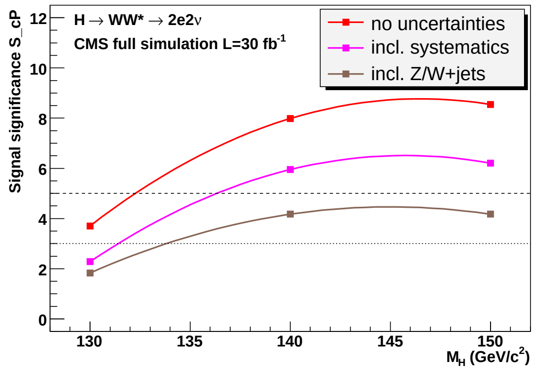

(a)

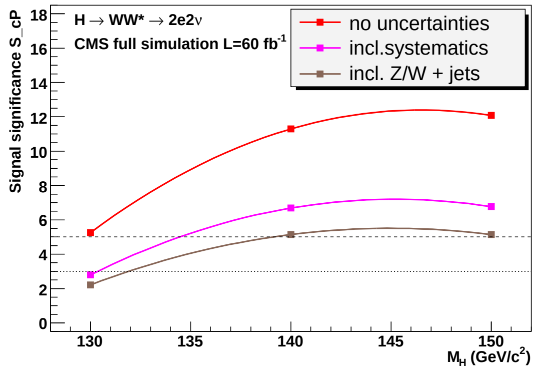

(b)

Figure 7: a) *Significance for 30* fb^{-1} *luminosity as function of the Higgs boson mass* M_{H} *with and without systematic uncertainties and expected* $\mathrm{W/Z + jet(s)}$ *background.* b) *Significance for 60* fb^{-1} *luminosity as function of the Higgs boson mass* M_{H}*, with the effect of the uncertainty on the theory, as well as experimental and luminosity systematics explicitly shown.*

devoted to the control of the $\mathrm{W/Z}$+jet(s) backgrounds. Electron isolation and identification is a crucial issue to avoid "fake" contributions to $\mathrm{e^+e^-}$ pairs in W+jet(s) events. Missing transverse momentum is caused by mismeasurements of jets in Z+jet(s) events. A dedicated cut strategy has been introduced to tame the W+jet(s) and Z+jet(s) background rates, by tightening electron identification and exploiting specific kinematic characteristics. These background sources have been suppressed to a manageable level. Theoretical and experimental systematics have been propagated to establish the sensitivity of the CMS experiment to the SM Higgs boson. A Higgs boson of $M_{\mathrm{H}} \gtrsim 134$ GeV$/c^2$ can be observed with a significance above 3 standard deviations in the $\mathrm{e^+\nu e^-\bar{\nu}}$ channel alone for an integrated LHC luminosity $\mathcal{L}$ above 30 fb^{-1}. This provides an excellent complementarity with the ZZ* channel [35].

A stand-alone discovery (above 5 standard deviations) can be established for masses in the range 139 to 150 GeV$/c^2$ for $\mathcal{L}$ above 60 fb^{-1}.

8 Acknowledgments

We would like to thank P. Busson, A. Nikitenko and I. Puljak for their interest in this $\mathrm{WW^{(*)}}$ *analysis and several useful discussions. Our thanks go also to the other members working on the* $\mathrm{H \to WW^{(*)} \to l\nu l\nu}$ *channel, G. Davatz, V. Drollinger, A.S. Giolo-Nicollerat and M. Zanetti for their collaboration and Prof.J.de Troconiz for his support.*

References

[1] The LEP Working Group for Higgs searches, ALEPH, DELPHI, L3 and OPAL collaborations, Phys. Lett. **B 565** (2003) 61.

[2] CDF and D0 Collaborations, *“Results of the Tevatron Higgs Sensitivity Study”*, **FERMILAB-PUB-03/320-E**

[3] M. Dittmar and H.K. Dreiner, *”How to find a Higgs boson with mass between 155 GeV to 180 GeV at the LHC”*, Phys.Rev. **D 55** (1997) 167 ;
M. Dittmar and H.K. Dreiner, *”LHC Higgs Search with $l^+\nu l^-\bar{\nu}$ final states”*, CMS NOTE-1997/083.

[4] G. Davatz, M. Dittmar, A.-S. Giolo-Nicollerat, *”Standard Model Higgs Discovery Potential of CMS in the* $\mathrm{H} \rightarrow \mathrm{WW} \rightarrow \mathrm{l}\nu\mathrm{l}\nu$ *Channel”*, CMS NOTE-2006/047.

[5] CMS Collaboration, *”The Compact Muon Solenoid - Technical Proposal”*, CERN/LHCC 94-38 (1994) 290.

[6] CMS Physics Technical Design Report, Volume 1, CERN-LHCC-2006-001 (2006)

[7] PYTHIA 6.215 is used for the Higgs signal and the WW, ZW, ZZ and $\mathrm{W/Z}$+jets backgrounds, PYTHIA 6.227 for $\mathrm{gg} \rightarrow \mathrm{WW}$
T Sjostrand *et al.*, Comput. Phys. Comm. **135** (2001) 238.

[8] TOPREX is used for the $\mathrm{t\bar{t}}$ and $\mathrm{Wt(b)}$ backgrounds
S.R. Slabospitsky, L. Sonnenschein, Comput. Phys. Comm. **148** (2002) 87.

[9] T. Binoth, M. Ciccolini, N. Kauer and M Kramer, JHEP **0503** (2005) 065.

[10] CMSIM133 is used for signal and backgrounds except $\mathrm{gg} \rightarrow \mathrm{WW}$(OSCAR365) http://cmsdoc.cern.ch/cmsim/cmsim.html.

[11] ORCA_8_7_3 is used for signal and background http://cmsdoc.cern.ch/orca.

[12] FAMOS_1_4_0 is used.
CMS Physics Technical Design Report, Volume 1, CERN-LHCC-2006-00 (2006) 55

[13] S. Frixione and B.R. Webber, *”Matching NLO QCD computations and parton shower simulations”*, JHEP **0206** (2002) 029; S. Frixione, P. Nason and B.R. Webber, *”Matching NLO QCD and parton showers in heavy flavour production”*, JHEP **0308** (2003) 007.

[14] G. Davatz, G. Dissertori, M. Dittmar, M. Grazzini and F. Pauss,
”Effective K-factors for $\mathrm{gg} \rightarrow \mathrm{H} \rightarrow \mathrm{WW} \rightarrow \mathrm{l}\nu\mathrm{l}\nu$ *at the LHC”*, JHEP **0405** (2004) 009.

[15] Higgs signal cross section calculation for the CMS Physics Technical Design Report by M. Spira.

[16] J. Pumplin *et al.*, J. High Energy Phys. 07 (2002) 47.

[17] A. Djouadi *et al.*, Comp. Phys. Comm. 108 (1998) 56.

[18] WW, WZ, ZZ and Z+jet cross section calculation for the CMS Physics TDR by J. Campbell using MCFM.

[19] M. Beneke *et al*, *“1999 CERN Workshop on Standard Model Physics (and more) at the LHC”*, CERN Yellow Report, **CERN-2000-04**

[20] J. Campbell and F. Tramontano, *”Next-to-leading order corrections to* Wt *production and decay”*;
Les Houches 2005 ”Physics at Tev Colliders 2005”, proceedings to be published.

[21] W+jet cross section by A.D. Martin, R.G. Roberts, W.J. Stirling and R.S. Thorne,
”Parton distributions for the LHC: W and Z production” Eur. Phys. J. **C 14** (2000) 133.

[22] S. Cucciarelli *et al.*, *”Track reconstruction, primary vertex finding and seed generation with the Pixel Detector”* CMS NOTE-2006/026 22.

[23] CMS Collaboration, “The Tracker Project - Technical Design Report”, CERN/LHCC 98-6 (1998) 625.; *idem*, ”Addendum to the Tracker TDR”, CERN/LHCC 2000-016 (2000) 82.

[24] CMS Collaboration, “The Electromagnetic Calorimeter Project - Technical Design Report”, CERN/LHCC 97-23 (1998) 364.

[25] E. Meschi *et al.*, *”Electron reconstruction in the CMS Electromagnetic Calorimeter”*, CMS NOTE-2001/034.

[26] S. Baffioni *et al.*, *”Electron Reconstruction in CMS”*, CMS NOTE-2006/040.

[27] R. Fruhwirth, Comp. Phys. Comm. 100 (1997) 1;
R. Fruhwirth *et al.*, Comp. Phys. Comm. 110 (1998) 80;
W. Adam *et al.*, *”Reconstruction of electrons with the Gaussian Sum Filter in the CMS Tracker at LHC”*, CMS NOTE-2005/001.

[28] Following the prescriptions of CMS PRS SC.

[29] V. Drollinger *et al.*, *”Modeling the Production of W pairs at LHC”*, CMS NOTE-2005/024.

[30] A. Cooper-Sakar *et al.*, Proceedings of the HERA/LHC Workshop 2004/2005.

[31] V. Büge *et al.* *”Prospects for the precision measurement of the W mass with the CMS detector at the LHC”*, CMS NOTE-2006/061.

[32] D. Acosta, *”Systematic uncertainties”*, talk CMS week, February 2006.

[33] Following the prescriptions of CMS PRS group. The significance is calculated using the ”scp” program, S.I. Bityukov and N.V. Krasnikov, Mod. Phys. Lett. A **13**, (1998) 3235.

[34] R. Fruhwirth, Nucl. Inst. Methods **A 262**(1987) 444.

[35] S. Baffioni et al., *”Discovery potential for the SM Higgs boson in the* $\mathrm{H} \rightarrow \mathrm{ZZ}^{(*)} \rightarrow \mathrm{e}^{+}\mathrm{e}^{-}\mathrm{e}^{+}\mathrm{e}^{-}$ *decay channel”*, CMS NOTE-2006/115.